Influence of Surface Irregularities on the Dynamic Response of Minor Highway Bridges

Nielsen, Søren R. K.; Kirkegaard, Poul Henning

Publication date:
1998

Document Version
Publisher's PDF, also known as Version of record

Stochastic Structural Dynamics, Spencer & Johnson (eds) © 1999 Balkema, Rotterdam, ISBN 90 5809 024 8

Influence of surface irregularities on the dynamic response of minor highway bridges

S.R.K. Nielsen & P.H. Kirkegaard
Department of Building Technology and Structural Engineering, Aalborg University, Denmark

ABSTRACT: In the present paper the effect on the dynamic amplification factor of bridge response from the surface irregularities is investigated. A numerical 3D model has been formulated for a 48t Scania truck. Further, a characteristic minor highway bridge has been selected, and a numerical FEM-model has been formulated. Based on measured data, a 2D spectral description of the road roughness is established which models the deterministic trends in transversal (wheel tracking) as well as longitudinal direction (some long-waved tendency). Further, the bumps/expansion joints at the approaches to the bridge are included into the model. Based on a Monte Carlo simulation study the mean value and the variational coefficient of several dynamic amplification factors have been calculated assuming the parameters describing the vehicle and the bridge deterministic at characteristic values. The overall conclusion from the study is that the most important impact on the magnitude of the dynamic amplification factor stems from short waved bumps.

1 INTRODUCTION

The determination of the dynamic response of a bridge resulting from the passage of a vehicle across the span is a problem of great interest which can be seen from the literature reviews given in (Kirkegaard et al. 1997a, Paultres et al. 1994). The forces that produce the stresses in a bridge under dynamic loading are a result of the dead load of the vehicle and the bridge and the vehicle -bridge interactive forces. The forces depend on many factors such as the natural frequencies and damping ratios of the vehicle and bridge, the vehicle suspension system, speed of vehicle, the traffic intensity and the road surface irregularities of the bridge deck (e.g. see Green et al. 1996, Inbanathan et al. 1988). Road surface irregularities have been measured in several studies (e.g. see Dodds et al. 1973, Honda et al. 1983, Marcondes 1992). It has been found that most pavement profiles have very similar power spectral densities and, further, by plotting the spectral densities versus the wave number in a double-logarithmic scale, it becomes obvious that all kinds of road pavements can be characterized by similar functions. This function may be approximated sufficiently by a straight line (Mathieu et al. 1991). Road surface roughness on bridges have been measured only rarely. Therefore, most studies done on the dynamic behavior of bridges have used the spectral densities, which have been found for road surface roughness. In the paper by Honda et al. (1982), the spectral densities of road surface roughness on bridges have been found to be modeled in the same manner as the spectrum of surface roughness on general roads. However, all the proposed spectral densities of road surface roughness are only one-dimensional, i.e. the spectral densities model only road profile in the longitudinal direction of the road and not in the transverse direction. The present paper establishes a 2D spectral description of the road roughness surface based on measurements from a Danish road. A part of the measured road includes a part of a bridge wherefore the irregularities due to the abutments also have been taken into the stochastic description of the road. The paper is organized in the following sections. Section 2 gives a description of the measured data. Next, in section 3, a model of a two-dimensional spectral density function of road surface roughness is given. Section 4, presents a Monte Carlo simulation study where the stochastic model is used to investigate the effect on the dynamic amplification factor of bridge response from the surface irregularities. At last, in sections 5 and 6, references and conclusions are given.

2 LASER-BASED MEASUREMENTS OF ROAD SURFACES

The measurements of the road irregularities considered in this paper have been obtained using a Profilograph.

2.1 *Presentation of the Measured Raw Data*

In 1991, the Danish Road Directorate introduced profilometric measurements of pavement surfaces by purchasing its first Profilograph. The concept of the Profilograph is a system with several lasers positioned on a vertical adjustable beam in front of a vehicle, measuring a point on the pavement surface at every 5 mm in the longitudinal direction. The pavement's transverse profile is measured in points according to the lasers position on the beam covering a maximum width of 3.5 meters. A data series obtained by the Profilograph with a measuring width of 3.2 meters has been provided by the Danish Road Directorate (see Schmidt et al. 1996). The data series are measured on the left side of the road Åsvej in the municipality of Roskilde on the island Zealand. Figure 1 shows the measured road profile after the mean values for each laser in longitudinal direction have been removed. In the longitudinal direction, estimates of the road irregularities are given for each 0.1 m, while in the transverse direction, estimates are given corresponding to the laser positions. It is seen that the measured road profile has large overall variations in the profiles together with the overall roughness. Figure 2 shows the measured road profile after these trends have been removed in the transversal direction. A typical wheel tracking pattern is seen. Next in figure 3 the Power Spectral Density (PSD) is shown versus the wave number in a double-logarithmic scale. It becomes obvious that the road irregularities can be approximated sufficiently by a straight line in this double-logarithmic scale. In order to investigate the surface roughness closer (wave lengths < 10 m) the measured data have been filtered using a 6'th order highpass digital elliptic filter with 0.5 decibels of ripple in the passband and a stopband 20 decibels down. Again, it became obvious that also the filtered road irregularities could be approximated sufficiently by a straight line in this double-logarithmic scale. However, it was seen that the slop for the filtered road profiles was smaller than for the unfiltered road profiles. Further, by considering figure 2 some more pronounced irregularities can be seen in the right side of the road at positions around 75 m and 125, respectively. These could be bumps/expansion joints at the approaches to the bridge.

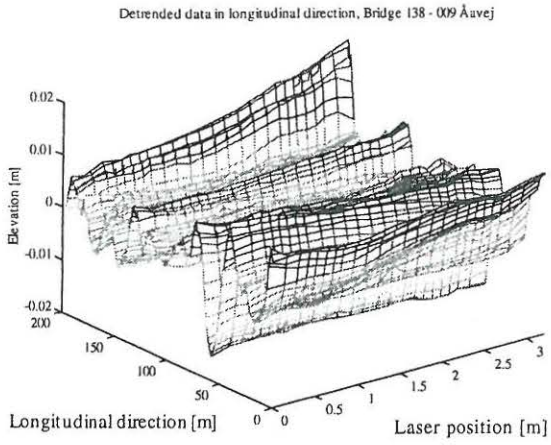

Figure 1. The measured road profile from bridge. Laser no 1 the left side of the road, laser no. 25 in the right side of the roa

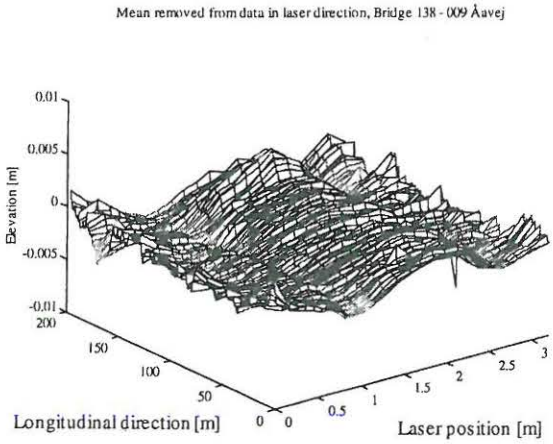

Figure 2 The measured road profile from bridge. Laser no 1 i the left side of the road, laser no. 25 in the right side of the roa Mean removed in longitudinal direction and in laser directior

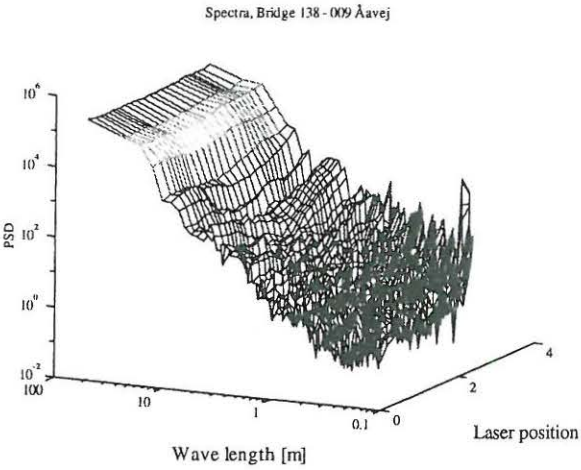

Figure 3 PSD of the measured road profile from bridge showi as a function of laser position and wave number in a doubl logarithmic mapping.

In order to investigate the correlation in transversal direction between the time series measured with the 25 lasers the sample correlation coefficient function has been estimated. The estimated correlation coefficient functions for different directions were compared and based on a visual comparison the surface is said to have properties which are covariance homogeneous and isotropic.

3 STOCHASTIC MODEL OF SURFACE IRREGULARITIES

The aim of the following section is to establish a stochastic model for the surface irregularities. This model will model, based on the observations from figures 1-3, the deterministic trends in transversal (wheel tracking) as well as longitudinal direction (some long-waved tendency). Further, the bumps/expansion joints at the approaches to the bridge and the stochastic nature of the surface roughness will be included into the model. The stochastic model presented is based on a (x_1,x_2,x_3)-coordinate system see figure 4 placed on a horizontal smooth base surface of the road. The x_1 - axis is directed along the longitudinal and the x_2 - axis along the transversal direction. The origo is placed at one side of the road, so $(x_1,x_2) \in]-\infty, \infty[\times [0, B]$. B indicates the width of the road.

The surface irregularities from the base line are modelled by the stochastic process $\{Z(x_1,x_2) \in [0, L] \times [0, B]\}$. This quantity is measured at N_2 discrete positions in the transverse direction equal to the number of lasers. In x_1 -direction the measurement points are sampled with the distance $\Delta x_1 = \frac{L}{N_1}$ where L is the measurement length and N_1 is the number of samples.

For $Z(x_1, x_2)$ the following model is applied

$$Z(x_1,x_2) = \mu_Z(x_1,x_2) + \sigma_Z(x_2)Y(x_1,x_2) \qquad (1)$$

$\mu_Z(x_1,x_2) = E[Z(x_1, x_2)]$ signifies the mean value function specifying the deterministic trends in the

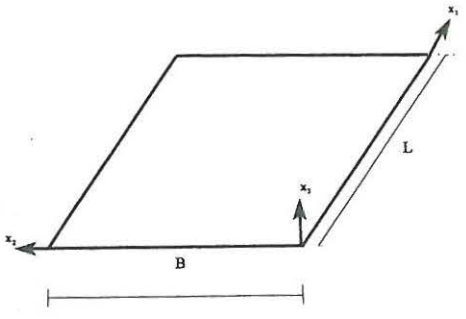

Figure 4 Geometry for stochastic model

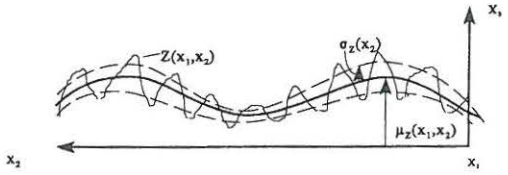

Figure 5 Graphical interpretation of $\mu_Z(x_1,x_2)$ and $\sigma_Z(x_2)$

surface irregularities due to small hills or other low frequency trends in the longitudinal direction, expansion joints at the abutments of the bridge and wheel tracking in the transverse direction. The standard deviation $\sigma_Z(x_2) = (E[(Z(x_1, x_2) - \mu_Z(x_1,x_2))^2])^{1/2}$ is a measure of the magnitude of the surface irregularities on the top of the deterministic trends. This quantity is assumed to be homogeneous in the longitudinal direction, i.e. corresponding to no x_1-depending. The variation is believed to be larger at the "hills" than in the "valleys" due to polishing from traffic as sketched in figure 5.

Finally, $\{Y(x_1,x_2) \in [0, L] \times [0, B]\}$ is a zero mean homogeneous isotropic Gaussian stochastic process with variance $\sigma^2_Y(x_1, x_2) \equiv 1$. The extend of low frequency trends and wheel tracking cannot be foreseen in advance. Hence $\mu_Z(x_1,x_2)$ and $\sigma_Z(x_2)$ should be considered as random variables generated by a number of basic variables entering the models of these quantities, which will be specified below. The indicated expectation for $\mu_Z(x_1,x_2)$ and $\sigma_Z(x_2)$ should then be interpreted as conditioned on these basic variables. The mean value function of the road surface is modelled as a sum of independent deterministic trends in the x_1 and x_2 direction, i.e. $\mu_Z(x_1,x_2) = \mu_Z^{(1)}(x_1,) + \mu_Z^{(2)}(x_2)$. The deterministic trend in the x_1-direction has been selected in figure 6a. Half-sine irregularities of amplitude B_1, B_2, B_1' and B_2' and the wave-length terms L_1, L_2, L_1' and L_2' are present on the approaches to the bridge. The distances between the irregularities are denoted L_0 and L_0', respectively. The irregularities with amplitudes B_2 and B_2' are modeling the expansion joints whereas the irregularities with amplitudes B_1 and B_1' are supposed to represent some long-waved tendency in the longitudinal road profile, i.e. $L_1, L_1' >> L_2, L_2'$. The basic variables L_0, L_1, L_2, B_1, B_2, L_0', L_1', L_2', B_1', B_2' are assumed to be mutually independent variables. L_0 and L_0' are identically Rayleigh-distributed, $L_0,L_0' \sim R(\sigma^2_{L_0})$. Similarly, $B_1,B_1' \sim R(\sigma^2_{B_1})$, $B_2,B_2' \sim R(\sigma^2_{B_2})$, $L_1,L_1' \sim R(\sigma^2_{L_1})$, $L_2,L_2' \sim R(\sigma^2_{L_2})$ are supposed to be pairwise identically distributed stochastic variables.

The model for $\mu_Z(x_2)$ has been sketched in figure 6b. Only the wheel-tracking in one lane is shown. $\mu_Z(x_2)$ is assumed to be symmetric around $x_2 = B/2$. The profile is defined by the heights A_0 and A_1, assuming a cubic

a)

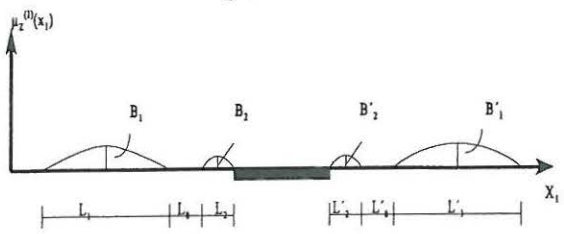

b)

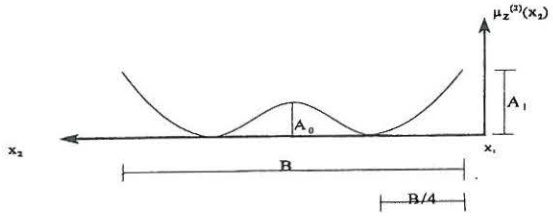

Figure 6a,b Model of mean-value function $\mu_Z(x_1,x_2) = \mu_Z^{(1)}(x_1,) + \mu_Z^{(2)}(x_2)$

spline between the node-points. Further, it is assumed that the term A_0 is deterministically related to A_1 according to

$$A_0 = \alpha_0 A_1 , \quad \alpha_0 \in [0,1] \tag{2}$$

$A_1 \sim R(\sigma^2_{A_1})$ is a Rayleigh-distributed random variable independent of the random variables generating the longitudinal profile $\mu_Z(x_1)$. The parameter α_0 is a deterministic decreasing function with age and traffic amount.The standard deviation in the transverse direction is modelled as shown in figure 7. Only one lane is shown and $\sigma_Z(x_2)$ *is* assumed to be symmetric around $x_2 = B/2$ as was the case for $\mu_Z(x_2)$. C_1 is assumed to represent the surface irregularities of the new laid road which is assumed to be Rayleigh-distributed $C_1 \sim R(\sigma^2_{C_1})$, and is assumed to be independent of the basic random variables generating $\mu_Z(x_1,x_2)$. C_0 and C_2 are reduced surface irregularities due to polishing. These are modelled as follows

$$\begin{aligned} C_0 &= \gamma_0 C_1 \qquad \gamma_0 \in [0,1] \\ C_2 &= \gamma_2 C_1 \qquad \gamma_2 \in [0,1] \end{aligned} \tag{3}$$

γ_0 and γ_2 are assumed to be deterministic decreasing functions of the ageing of the pavement and the traffic amount.

Initially, samples of $\mu_Z(x_1,x_2)$ and $\sigma_Z(x_2)$ are generated upon generating independent samples of the quantities entering the models of these quantities. Assuming a

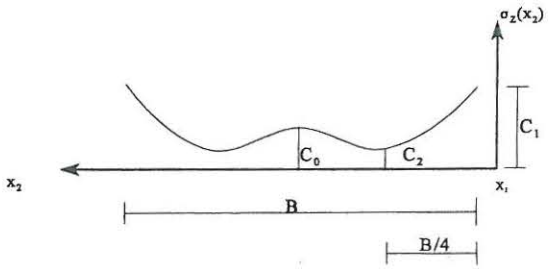

Figure 7 Model of standard deviation $\sigma_Z(x_2)$

realization $y(x_1,x_2)$ of the field $\{Y(x_1,x_2)\}$ is available, realizations of the road surface then become $Z(x_1,x_2) = \mu_Z(x_1,x_2) + \sigma_Z(x_2)\, y(x_1,x_2)$, cf. (1).

In order to calculate realizations of the stochastic field $\{Y(x_1,x_2) \in [0, L] \times [0, B]\}$ the following stochastic model is applied

$$\begin{aligned} Y(x_1,x_2) = \sum_{m=1}^{N_1}\sum_{n=1}^{N_2} A_{mn}\cos\left[2\pi\left(m\frac{x_1}{L}+n\frac{x_2}{B}\right)-\Phi_{mn}\right] + \\ B_{mn}\cos\left[2\pi\left(m\frac{x_1}{L}-n\frac{x_2}{B}\right)-\Psi_{mn}\right] \end{aligned} \tag{4}$$

In (4) $A_{mn} \sim R(\sigma^2_{A_{mn}})$ and $B_{mn} \sim R(\sigma^2_{B_{mn}})$ are Rayleigh distributed random variables with the parameters $\sigma^2_{A_{mn}}$ and $\sigma^2_{B_{mn}}$, and $\Phi_{mn} \sim U(0,2\pi)$, $\Psi_{mn} \sim U(0,2\pi)$ are uniformly distributed over the interval $[0, 2\pi]$. All the random variables A_{mn}, B_{mn}, and Φ_{mn}, Ψ_{mn} in (4) are mutually independent. If $A \sim R(\sigma^2)$ and $\Phi \sim U(0,2\pi)$ it is well-known that $X = A\cos(x - \Phi)$ becomes normal distributed with zero mean and variance σ^2, i.e $X \sim N(0,\sigma^2)$. Hence, (4) consists of a sum of mutually independent zero mean independent normal variables. $\{Y(x_1,x_2)\}$ is then a zero mean Gaussian process from the various mixing theorems generalizing the central limit theorem to stochastic processes. The auto-covariance function of (4) becomes

$$\begin{aligned} \kappa_{YY}(\xi_1,\xi_2) = E[Y(x_1,x_2)Y(x_1+\xi_1,x_2+\xi_2)] \approx \\ \sum_{m=1}^{N_1}\sum_{n=1}^{N_2}\left[\sigma^2_{A_{mn}}\cos\left(2\pi(m\frac{\xi_1}{L}+n\frac{\xi_2}{B})\right)+\sigma^2_{B_{mn}}\cos\left(2\pi(m\frac{\xi_1}{L}-n\frac{\xi_2}{B})\right)\right] \end{aligned} \tag{5}$$

The straight forward insertion of (4) into the left -hand side of (5) results in a four-double sum. However, only the diagonal terms in this four-double sum retains, using the mutual independence of the involved stochastic variables. The homogeneity of $\{Y(x_1,x_2)\}$ follows from the last statement of (5). The following 2-dimensional Fourier transformation applies

$$\left.\begin{aligned}\kappa_{YY}(\xi_1,\xi_2) &= \int_{-\infty}^{\infty}\int_{-\infty}^{\infty} e^{i(\xi_1 k_1+\xi_2 k_2)} S_{YY}(k_1,k_2)dk_1dk_2 \\ S_{YY}(k_1,k_2) &= \frac{1}{4\pi^2}\int_{-\infty}^{\infty}\int_{-\infty}^{\infty} e^{-i(\xi_1 k_1+\xi_2 k_2)} \kappa_{YY}(\xi_1,\xi_2)d\xi_1 d\xi_2\end{aligned}\right\} \quad (6)$$

(6) is known as the so-called Wiener - Khintchine relations. $S_{YY}(k_1,k_2)$ is termed the auto-spectral density of the surface irregularities process $\{Y(x_1,x_2)\}$. Since, both $S_{YY}(k_1,k_2)$ and $\kappa_{YY}(\xi_1,\xi_2)$ are real, the imaginary parts of $e^{\pm i(\xi_1 k_1+\xi_2 k_2)}$ cancel, and may be replaced by cos $(\xi_1 k_1+\xi_2 k_2)$. The first part of (6) can then be written

$$\begin{aligned}&\kappa_{YY}(\xi_1,\xi_2) = \int_{-\infty}^{\infty}\int_{-\infty}^{\infty}\cos(k_1\xi_1+k_2\xi_2)S_{YY}(k_1,k_2)dx_1dx_2 = \\ &\int_0^{\infty}\int_0^{\infty}\Big[2\cos(k_1\xi_1)\cos(k_2\xi_2)\Big(S_{YY}(k_1,k_2)+S_{YY}(-k_1,k_2)\Big)dk_1dk_2 - \\ &2\sin(k_1\xi_1)\sin(k_2\xi_2)\Big(S_{YY}(k_1,k_2)-S_{YY}(-k_1,k_2)\Big)dk_1dk_2\Big] \approx \\ &\sum_{m=1}^{N_1}\sum_{n=1}^{N_2}\Big[2\cos\Big(2\pi m\frac{\xi_1}{L}\Big)\cos\Big(2\pi n\frac{\xi_2}{B}\Big)\Big(S_{YY}(m\Delta k_1,n\Delta k_2)+ \\ &S_{YY}(-m\Delta k_1,n\Delta k_2)\Big)\Delta k_1\Delta k_2 - 2\sin\Big(2\pi m\frac{\xi_1}{L}\Big)\sin\Big(2\pi n\frac{\xi_2}{B}\Big) \\ &\Big(S_{YY}(m\Delta k_1,n\Delta k_2) - S_{YY}(-m\Delta k_1,n\Delta k_2)\Big)\Delta k_1\Delta k_2\Big]\end{aligned} \quad (7)$$

where

$$\Delta k_1 = \frac{2\pi}{L} \quad , \quad \Delta k_2 = \frac{2\pi}{B} \quad (8)$$

Upon comparison (5) and (7) the following expressions are obtained for the parameters $\sigma^2_{A_{mn}}$ and $\sigma^2_{B_{mn}}$

$$\left.\begin{aligned}\sigma^2_{A_{mn}} &= 2S_{YY}(m\Delta k_1,n\Delta k_2)\Delta k_1\Delta k_2 \quad , \quad m=1,\ldots,N_1 \\ \sigma^2_{B_{mn}} &= 2S_{YY}(-m\Delta k_1,n\Delta k_2)\Delta k_1\Delta k_2 \quad , \quad n=1,\ldots,N_2\end{aligned}\right\} \quad (9)$$

Assuming $S_{YY}(k_1,k_2)$ to be known, the application of (4) can now be explained in the following steps:

1) Initially, the parameters $\sigma^2_{A_{mn}}$ and $\sigma^2_{B_{mn}}$ are calcula ted from (9).

2) For all (m,n) generate independent samples of the Rayleigh distributed random variables $A_{mn} \sim R(\sigma^2_{A_{mn}})$ and $B_{mn} \sim R(\sigma^2_{B_{mn}})$ as well as the mutually independent uniformly distributed variables $\Phi_{mn} \sim U(0,2\pi)$, $\Psi_{mn} \sim U(0,2\pi)$ by means of a random generator.

3) The corresponding realizations $y(x_1,x_2)$ of $\{Y(x_1,x_2)\}$ are calculated by (4).

Assuming a one-sided one-dimensional auto-spectrum $s_Y(k)$ of the surface irregularities is known from measurements and the field $\{Y(x_1,x_2)\}$ is assumed to be known, a relationship between $S_{YY}(k_1,k_2)$ and $s_Y(k)$ has to be established. The one-dimensional auto-covariance function for surface irregularities along the x_1 - axis for a fixed x_2 becomes

$$k_{YY}(\xi_1) = E[Y(x_1,x_2)Y(x_1+\xi_1,x_2)] = \kappa_{YY}(\xi_1,0) \quad (10)$$

Similar to (6) this function admits the mutual Fourier transforms

$$\left.\begin{aligned}k_{YY}(\xi) &= \int_{-\infty}^{\infty} e^{i\xi k}s_{YY}(k)dk \\ s_{YY}(k) &= \frac{1}{2\pi}\int_{-\infty}^{\infty} e^{-i\xi k}k_{YY}(\xi)d\xi\end{aligned}\right\} \quad (11)$$

$s_{YY}(k) = s_{YY}(-k) = s^*_{YY}(k)$ signifies the double-sided one-dimensional auto-spectrum. This is related to the two-dimensional auto-spectrum defined in as follows

$$s_{YY}(k) = \int_{-\infty}^{\infty} S_{YY}(k,k_2)dk_2 \quad (12)$$

Due to the symmetry properties $k_{YY}(\xi) = k_{YY}(-\xi)$ and $s_{YY}(k) = s_{YY}(-k)$, (12) can be replaced by the mutual cosine-transforms

$$\left.\begin{aligned}k_{YY}(\xi) &= \int_0^{\infty}\cos(k\xi)s_Y(k)dk \\ s_Y(k) &= \frac{2}{\pi}\int_0^{\infty}\cos(k\xi)k_{YY}(\xi)d\xi\end{aligned}\right\} \quad (13)$$

$$s_Y(k) = 2s_{YY}(k) \quad , \quad k>0 \quad (14)$$

Instead of the (x_1,x_2) coordinate system an arbitrary rotated (x'_1,x'_2) system is considered, see figure 8

Now, $S'_{YY}(k'_1,k'_2)$ signifies the auto-spectrum measured in the rotated coordinate system. If $S'_{YY}(k'_1,k'_2) = S_{YY}(k'_1,k'_2)$ the random Gaussian field is termed isotropic. In this case $S_{YY}(k_1,k_2)$ only depends

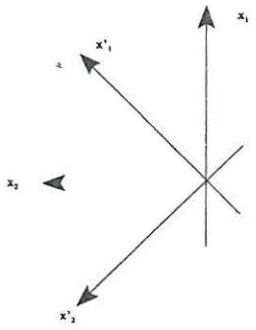

Figure 8 Definition of rotated coordinate system

on k_1 and k_2 via the magnitude $k = |\mathbf{k}| = (k_1^2 + k_2^2)^{\frac{1}{2}}$ of the wave-number vector, i.e. $S_{YY}(k_1,k_2) = S_{YY}(k)$. Based on the analysis in section 2 such an assumption may be adopted for the present field. Similarly, the auto-covariance function $\kappa_{YY}(\xi_1,\xi_2)$ does only depend on the separation distance $\xi = |\boldsymbol{\xi}|$ between the coordinate points, i.e. $\kappa_{YY}(\xi_1,\xi_2) = \kappa_{YY}(\xi)$. Upon evaluation the auto-spectrum in polar coordinates one has

$$
\begin{aligned}
S_{YY}(k) &= \frac{1}{4\pi^2}\int_0^{\infty}\int_0^{2\pi}\kappa_{YY}(\xi)e^{-ik\cdot\xi}\xi d\xi d\phi \\
&= \frac{1}{4\pi^2}\int_0^{\infty}\xi\kappa_{YY}(\xi)\int_0^{2\pi}\cos(k\xi\cos\phi)d\phi d\xi \\
&= \frac{1}{2\pi}\int_0^{\infty}\xi J_0(k\xi)k_{YY}(\xi)d\xi
\end{aligned}
\qquad (15)
$$

where ϕ is the angle between the vectors $\boldsymbol{\xi}$ and $\boldsymbol{k}$, and $J_0(x)$ is the Bessel function of zero order and 1st kind. $\kappa_{YY}(\xi)$ specifies the covariance between 2 points with the spacing ξ, and is in principle equal to the measured one-dimensional auto-covariance function $k_{YY}(\xi)$. Hence, (15) provides a relation between the two-dimensional auto-spectrum of an isotropic field and the one-dimensional auto-covariance function. (15) shows that $k_{YY}(\xi)$ and $2\pi\ S_{YY}(k)$ are mutual Hankel transforms. The inverse relation then reads

$$
k_{YY}(\xi) = 2\pi\int_0^{\infty} kJ_0(k\xi)S_{YY}(k)dk \qquad (16)
$$

Assume that $k_{YY}(\xi)$ can be written

$$
\left.
\begin{aligned}
k_{YY}(\xi) &= \sum_{j=1}^{J} c_j e^{-d_j\xi}\cos(e_j\xi) \\
\sum_{j=1}^{J} c_j &= 1
\end{aligned}
\right\} \qquad (17)
$$

where c_j, d_j and e_j are real constants. Then (15) becomes

$$
S_{YY}(k) = \frac{1}{2\pi}Re\left(\sum_{j=1}^{J} c_j\frac{p_j}{(k^2 + p_j^2)^{3/2}}\right),\ p_j = d_j + ie_j \qquad (18)
$$

At the derivation of (18) the following version of the Lipschitz integral has been used , Watson (1966)

$$
\begin{aligned}
&\int_0^{\infty}\xi J_0(k\xi)e^{-d\xi}\cos(e\xi)d\xi = Re\left(\int_0^{\infty}\xi J_0(k\xi)e^{(-d+ie)\xi}d\xi\right) = \\
&Re\left(\sum_{j=1}^{J} c_j\frac{p_j}{(k^2 + p_j^2)^{3/2}}\right),\quad p_j = d_j + ie_j
\end{aligned}
\qquad (19)
$$

(18) is the expression for $S_{YY}(k_1,k_2)$ searched for.

4 EXAMPLE

The proposed stochastic model for the surface irregularities has been used in a study of the effect on the dynamic amplification factor of bridge response from the surface irregularities. A numerical 3D model has been formulated for a 48t Scania truck. Further, a charateristic minor highway bridge has been selected, and a numerical FEM-model has been formulated, see (Kirkegaard et al. 1998) for details. Based on a Monte Carlo simulation study the mean value and the variational coefficient of dynamic amplification factors have been calculated assuming the parameters describing the vehicle and the bridge deterministic at characteristic values.

First, the expression in eq. (17) is fitted to the mean of the three correlation coefficient functions at points laying on a line in the transversal direction, the longitudinal direction and with an angle of 45 degrees, respectively. This calculation is performed using *constr.m* from the MATLAB Optimization Toolbox, Mathworks. Next a realization $y(x_1,x_2)$ of the field $\{Y(x_1,x_2)\}$ is calculated as described in section 3. A realization $y(x_1,x_2)$ of the field $\{Y(x_1,x_2)\}$ is then obtained from eq.(1) using the values of the basic varibles in table 1 and the models of the mean-value function and standard deviation given in figures 6 and 7, respectively.

An PSD obtained using the values in table 3.1 have been shown to model the PSD of the measured data very well, see (Kirkegaard et al. 1997b).

In the simulation study following simulation scenarios have been considered for a 48t Scania truck

Table 1 Statistical characteristics of basic variables.

Basic Variabel (X)	*Distribution*	*Standard Deviation (σ_X)*
Wave length (L_1)	Rayleigh	50.0 m
Wave length (L_2)	Rayleigh	0.50 m
Wave length (L_1')	Rayleigh	50.0 m
Wave length (L_2')	Rayleigh	0.50 m
Distance (L_0)	Rayleigh	10.0 m
Distance (L_0')	Rayleigh	10.0 m
Amplitude (B_1)	Rayleigh	0.01 m
Amplitude (B_2)	Rayleigh	0.002 m
Amplitude (B_1')	Rayleigh	0.01 m
Amplitude (B_2')	Rayleigh	0.002 m
Scale factor (α_0)	Deterministic	8
Scale factor (γ_0)	Deterministic	6
Scale factor (γ_2)	Deterministic	3
Profile height (A_1)	Deterministic	0.003 m
Irregularity height (C_1)	Deterministic	0.001 m

Table 2 Mean and COV results for simulation scenario 1.

Speed (km/h)	DAF of moment at mid-span	DAF of moment at intermediate support	DAF of shear force at end support
50	1.024 (0.21 %)	1.023 (0.21 %)	1.012 (0.20 %)
90	1.064 (0.44 %)	1.054 (0.42 %)	1.041 (0.15 %)

Table 3 Mean and COV results for simulation scenario 2.

Speed (km/h)	DAF of moment at mid-span	DAF of moment at intermediate support	DAF of shear force at end support
50	1.008 (0.80 %)	1.010 (0.45 %)	1.022 (0.51 %)
90	1.084 (2.36 %)	1.077 (2.34 %)	1.063 (2.13 %)

Scania vehicle acting on the bridge (speed = 50 and 90 km/h):

1) Only roughness (second part of (1)) is considered.

2) Only bumps (first part of (1)) is considered.

3) Bumps and roughness are considered.

4) Bumps and roughness are considered and the truck is moving 1 m in the transversal direction.

For each simulation the dynamic amplification of the maximum total moment in the longest span of the bridge, the total moment over the intermediate columns and the total maximum shear force at the supports have been estimated. The dynamic amplification factor (DAF) is taken as the ratio of the maximum total response and the static response. The mean value and the coefficient of variation (COV) of the DAF of the different response quantities have been estimated for 50 crossings. Tables 2, 3, 4 and 5 show the results for the different scenarios, respectively. It is seen that the obtained DAFs are relatively small. However, the mean value of the DAFs compares very well with the results from the literature, see e.g. (Kirkegaard et al. 1997a) and (Kirkegaard et al. 1998). The tables show that the most important impact on the magnitude of the dynamic amplification factor stems from short waved bumps. Further, it is seen that the DAFs are unchanged when the truck does not move in a straight path over bridge (scenario 4).

5 CONCLUSION

The present paper establishes a two-dimensional spectral description of the road roughness surface based on measurements from a Danish road where the deterministic trends in transversal (wheel tracking) as well as longitudinal direction (some long-waved tendency) is modeled. Further, the bumps/expansion joints at the approaches to the bridge and the stochastic nature of the surface roughness are included into the model. Based on a Monte Carlo simulation study the mean value and the variational coefficient of several dynamic amplification factors

Table 4 Mean and COV results for simulation scenario 3.

Speed (km/h)	DAF of moment at mid-span	DAF of moment at intermediate support	DAF of shear force at end support
50	1.015 (1.03 %)	1.011 (0.45 %)	1.021 (0.56 %)
90	1.099 (2.42 %)	1.077 (2.34 %)	1.063 (2.53 %)

Table 5 Mean and COV results for simulation scenario 4.

Speed (km/h)	DAF of moment at mid-span	DAF of moment at intermediate support	DAF of shear force at end support
50	1.021 (1.43 %)	1.019 (1.17 %)	1.022 (1.38 %)
90	1.086 (2.06 %)	1.078 (2.07 %)	1.064 (1.95 %)

have been calculated assuming the parameters describing the vehicle and the bridge deterministic at characteristic values. The overall conclusion from the study is that the most important impact on the magnitude of the dynamic amplification factor stems from short waved bumps.

ACKNOWLEDGEMENT

The present research was partially supported by The Danish Technical Research Council within the projects: *Dynamic amplification factor of vehicle loadings on smaller bridges* and *Damping Mechanisms in Dynamics of Structures and Materials.*

REFERENCES

Dodds, C.J., & J.D. Robson 1973. The description of Road Surface Roughness. *J. Sound and Vibration*, 31:175-183.

Green, M.F. & D. Cebon 1994. Dynamic Response of Highway Bridges to Heavy Vehicle Loads: Theory and Experimental Validation. *Journal of Sound & Vibration*. 170: 51-78.

Honda, H., Y. Kajikawa & T. Kobori 1982. Spectra of Road Surfaces Roughness on Bridges. *ASCE ST9*. 108: 1956-1966.

Inbanathan, M.J. & M. Wieland 1987. Bridge Vibrations due to Vehicle Moving over Rough Surface. *Journal of Structural Engineering. ASCE*. 113: 1994-2008.

Kirkegaard, P.H., S.R.K. Nielsen & I. Enevoldsen 1997a. Heavy Vehicle on Minor Highway Bridge, A literature Review, *Sturctural Reliability Theory, Paper No. 169, Aalborg University*.

Kirkegaard, P.H., S.R.K. Nielsen & I. Enevoldsen 1997b. Heavy Vehicle on Minor Highway Bridge - Stochastic Modelling of Surface Irregularities. *Sturctural Reliability Theory, Paper No. 170, Aalborg University*.

Kirkegaard, P.H. & S.R.K. Nielsen 1998. Influence of Uncer tainty of Vehicle Dynamics on the Dynamic Response of Minor Highway Bridges. *Proc. of the Stochastic Structure Dynamics SSD'98 Conference, Notre Dame*.

Marcondes, J., G.J. Burgess & R. Harichandran 1991. Spectral Analysis of Highway Pavement Rougness. *Journal of Transportation Engineering*. 117: 110-122.

Mathieu, H., J.A. Calgaro & M. Prat 1991. Concerning Develop ment of Models of Traffic Loading and Rules for the Specification of Bridge Loads. *Final Report to the Commis sion of the European Communities on Contract No. PR2/90/7750/RN/46*.

Paultre, P., O. Chaallal & J. Proulx 1992. Bridge Dynamics and Dynamic Amplification Factors - Review of Analytical and Experimental Findings. *Canada Journal of Civil Engineer ing*.19: 260-278.

Schmidt, B. & A.Taudorf 1996. *Experiences in using Profilograph, A laser-Based Equipment for Profilmetric Measurements of Pavement Surface.*

Watson, G.N. 1966. *A Treatise of the Theory on Bessel Func tions*. Cambridge at the University Press, 1966.